Journal Pre-proof

Simultaneous removal of Cr(III) and V(V) and enhanced synthesis of high-grade rutile TiO_2 based on sodium carbonate decomposition

Guo Chen, Qi Jiang, Kangqiang Li, Aoxi He, Jinhui Peng, Mamdouh Omran, Jin Chen

PII: S0304-3894(20)30025-X

DOI: https://doi.org/10.1016/j.jhazmat.2020.122039

Reference: HAZMAT 122039

To appear in: *Journal of Hazardous Materials*

Received Date: 23 October 2019

Revised Date: 1 January 2020

Accepted Date: 6 January 2020

Please cite this article as: Chen G, Jiang Q, Li K, He A, Peng J, Omran M, Chen J, Simultaneous removal of Cr(III) and V(V) and enhanced synthesis of high-grade rutile TiO_2 based on sodium carbonate decomposition, *Journal of Hazardous Materials* (2020), doi: https://doi.org/10.1016/j.jhazmat.2020.122039

Simultaneous removal of Cr(III) and V(V) and enhanced synthesis of high-grade rutile TiO_2 based on sodium carbonate decomposition

Guo Chen [a, b], Qi Jiang [b], Kangqiang Li [a, b, 1], Aoxi He [a, b, **], Jinhui Peng [a, b], Mamdouh Omran [d], Jin Chen [a, b , c, *]

[a] *Key Laboratory of Green-Chemistry Materials in University of Yunnan Province, Kunming Key Laboratory of Energy Materials Chemistry, Yunnan Minzu University, Kunming 650500, P.R. China.*

[b] *Key Laboratory of Unconventional Metallurgy, Ministry of Education, Kunming University of Science and Technology, Kunming 650093, P.R. China.*

[c] *State Key Laboratory of Vanadium and Titanium Resources Comprehensive Utilization, Pangang Group Research Institute Co., Ltd., Panzhihua 617000, P.R. China.*

[d] *Process Metallurgy Research Group, Faculty of Technology, University of Oulu, Finland.*

[*] Corresponding author: Tel: +86-871-65910017; Fax: +86-871-65910017

E-mail address: realchenguo@aliyun.com

[**] Co-corresponding author: Tel: +86-871-65910017; Fax: +86-871-65910017

E-mail address: yan9249@vip.qq.com

[1] These authors contributed equally to this work and should be regarded as co-first authors.

Graphical Abstract

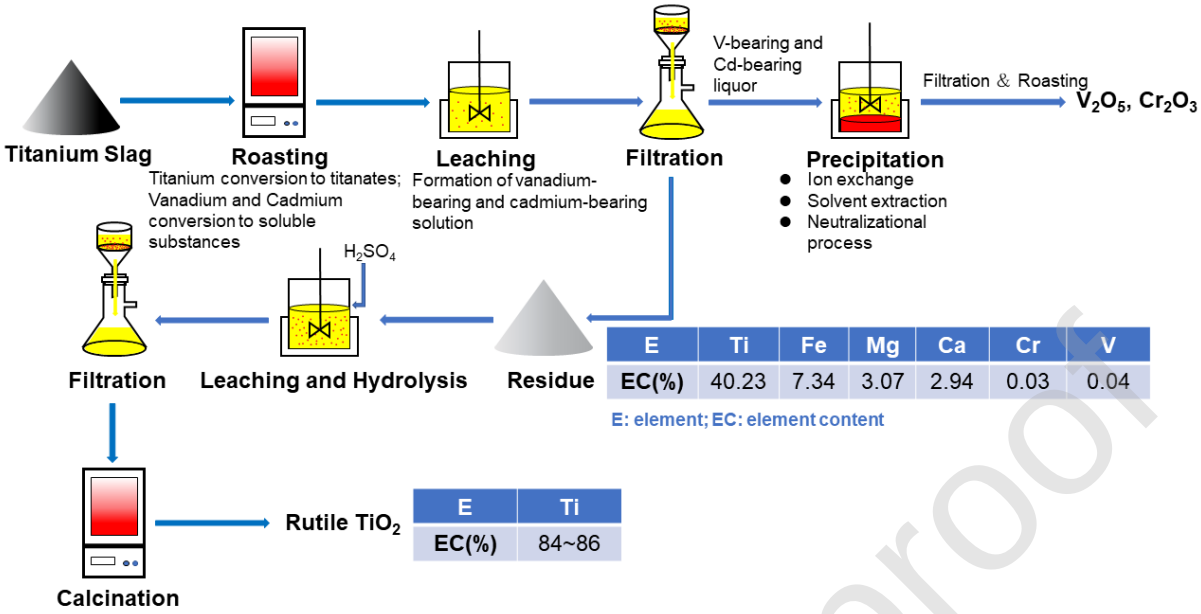

E	Ti	Fe	Mg	Ca	Cr	V
EC(%)	40.23	7.34	3.07	2.94	0.03	0.04

E: element; EC: element content

E	Ti
EC(%)	84~86

Proposed processes for recovering vanadium (V) and chromium (Cr) and simultaneously preparing rutile TiO_2.

Highlights

- *Removal of Cr(III) and V(VI) from titanium slag for enhanced synthesis of TiO_2.*
- ΔG^{θ} for sodium carbonate decomposition reactions were deduced.
- Sodium carbonate can be applied effectively for pretreatment of minerals.
- *Rutile TiO_2 has been synthesized successfully.*

Abstract

Rutile TiO_2 is widely applied as the raw material to produce titanium dioxide and titanium sponge, whereas the Cr (Ⅲ) and V (V) impurities in rutile TiO_2 significantly affect the performance of related products. In the present work, the sodium carbonate decomposition treatment on Panzhihua titanium slag was attempted, to improve the preparation process of rutile TiO_2 with high crystallinity and simultaneously reduce the chromium (Cr) and vanadium (V) content as hazardous elements. Effects of sodium carbonate decomposition treatment on the crystal composition, microstructure of rutile TiO_2 were determined using XRD, SEM and Raman characterization. The recovery of Cr(Ⅲ) and V(V) was achieved through leaching the roasted titanium slag by dilute sulfuric acid, with the chromium and vanadium content in the residue decreasing up to 0.03 % and 0.04 %, respectively, followed by the final product rutile TiO_2 was produced by the leaching residue calcined at 1323.15 K with a duration time of 120 min, with 85.56 % of TiO_2 grade. The work highlights the feasibility of synchronously preparing rutile TiO_2 and removing hazardous Cr (Ⅲ) and V (V) impurities from titanium slag using sodium carbonate decomposition.

Keywords: titanium slag; chromium; vanadium; rutile TiO_2; sodium carbonate decomposition

1. Introduction

The vanadium-titanium magnetite resources in Panzhihua City (Sichuan Province, P.R. China) are abundant, containing various valuable elements such as Fe, Ti, Cr, V, Co and Ni (Chen et al., 2013; Dong et al., 2012; Xiang et al., 2017). Moreover, Panzhihua titanium slag

is mainly produced by electric furnace smelting method with the local ilmenite as the raw material. After electric furnace smelting, titanium occurs in the form of TiO_2, Ti_2O_3 and Ti_3O_5, and iron occurs as $FeTi_2O_5$ and metallic iron. Meanwhile, Panzhihua titanium slag contained a multitude of phases, including anosovite phase, glassy silicate containing V, Cr, Ca, Si and Al elements, rutile TiO_2, etc. (Huang et al., 2012a; Huang et al., 2013b; Zhao et al., 2014). The impurities in ilmenite are reduced to a certain extent after the smelting treatment, including Cr_2O_3, V_2O_5, MgO, MnO, Al_2O_3, CaO, SiO_2, P and S (Eriksson et al., 1996; Guéguin et al., 2007; Guo et al., 2014). From the thermomechanical analysis, these impurities are difficultly reduced, and gradually remain in titanium slag and further combined with low valence titanium to form complex compounds. Additionally, Rutile TiO_2 is widely applied as nanomaterials, ceramics materials, electronic materials (Hearne et al., 2004; Kaviyarasu et al., 2017; Kaviyarasu and Kennedy, et al., 2016), whereas the Cr(Ⅲ) and V(V) impurities in rutile TiO_2 significantly affect the performance of related products. Especially, hexavalent chromium (Cr^{6+}) is more toxic than trivalent chromium (Cr^{3+}), which are mainly attributed to those parts: structural similarity between sulphate and chromate is responsible for entrance of chromate into the cell; and in biological PH, trivalent chromium (Cr^{3+}) undergoes precipitation as hydroxide but hexavalent chromium (Cr^{6+}) remains in the solution; additionally, hexavalent chromium is labile center, with the symmetrical electronic configuration of the central ion being t2g0eg0, but trivalent chromium is inert, with the symmetrical electronic configuration of the central ion being t2g3eg0 (Saha and Nandi, 2011; Saha et al., 2013). It should be avoided for the oxidation behavior of trivalent chromium (Cr^{3+}) to hexavalent chromium (Cr^{6+}), otherwise there will cause enormous environmental problems.

Therefore, the efficient recovery of vanadium (V) and chromium (Cr) hazardous elements from titanium slag can render significant improvement to the environmental quality of titanium slag for subsequent usage.

Titanium (Ti) is dispersed in nature and difficult to extract, hence being considered to be a rare metal, which has been widely applied in pigment, catalyst, alloy, paper, corrosion resistant chemical material (Chen et al., 2010; Grätzel, 2003; Liu et al., 2013); meanwhile, titanium compounds are popularly utilized in coating, adsorbent, cosmetic and filler, etc. (Samal et al., 2009; Zhang and Nicol, 2010). Furthermore, titanium dioxide and titanium sponge are mainly prepared from rutile TiO_2, while the components of Panzhihua titanium slag are complicated, and the contents of Cr(Ⅲ) and V(V) impurities in rutile TiO_2 are high, which render a significant impact on the performance of titanium dioxide and titanium sponge. Therefore, it is meaningful and increasingly urgent to develop an effective and environmental benign method for the simultaneous removal of Cr(III) and V(V) impurities and enhanced synthesis of high-grade rutile TiO_2 from titanium slag.

The process of upgrading method for rutile TiO_2 product is usually reported as follows: titanium slag was firstly decomposed, and then the impurities were removed in subsequent leaching stages, followed by hydrolysis and calcination process to synthesize rutile TiO_2. Many methods have been developed for the beneficiation of titanium slag. Nayl et al. used ammonium hydroxide to manufacture titanium oxide with a high purity, and reported that ammonium titanite was formed through ilmenite roasted with ammonium hydroxide, followed by that ilmenite were hydrolyzed in hot water to be converted into anatase TiO_2 (Nayl et al., 2009). Alternatively, Liu et al. used a sodium-oxidization process to prepare high-grade rutile

TiO_2 pigment with 97.0 % purity from titanium slag, having high contents of Mg, Al, Si (Liu et al., 2015). Lasheen et al. proposed a soda ash roasting method to synthesize rutile TiO_2, wherein titanium slag was decomposed by Na_2CO_3 at high temperatures to form the intermediate $NaFeTiO_4$; followed by the intermediate was subjected to water leaching and dilute hydrochloric acid to form rutile TiO_2 (Lasheen et al., 2008). In summary, earlier works dissolved titanium slag with additives, indicating the destruction of titanium slag's refractory nature enabled it to improve the leaching behavior. Moreover, some processes also enabled watering leaching prior to acid leaching for Cr(Ⅲ) and V(V) removal, while few detailed studies have reported the effects of experimental leaching factors on the removal of Cr(Ⅲ) and V(V) from titanium slag. Furthermore, if the excellent characteristics of microwave heating were utilized to replace traditional heating in the proposed process (Li et al., 2019a; Li et al., 2019b; Li et al., 2019c; Li et al., 2020a; Li et al., 2020b; Li et al., 2020c; Li et al., 2020d), including roasting and calcination, the merits of the process would be much advantageous.

In this work, a highly efficient process by sodium carbonate roasting-leaching was proposed to produce high-grade rutile TiO_2 and simultaneously recover Cr(Ⅲ) and V(V) from Panzhihua titanium slag. Experimental parameters affecting the quality index of rutile TiO_2 and removal degree of Cr(Ⅲ) and V(V) were investigated and optimized, and the recovery process of Cr(Ⅲ) and V(V) were proposed. Furthermore, effects of experimental factors in the proposed method on the crystal compositions, microscopic appearance of titanium slag were systematically investigated, including Na_2CO_3/slag mass ratio, roasting temperature and roasting time.

2. Experimental

2.1 Materials

Titanium slag as the studied raw material was received from Panzhihua Iron and Steel Research Institute (Panzhihua city, Sichuan Province, P.R. China). Table1 listed the chemical analysis of raw titanium slag, and indicated that Panzhihua titanium slag contained low-grade TiO_2 (71.82%) and high-content impurities such as Cr, V, Mg, and Fe. In addition, the phase compositions of raw titanium slag were displayed in Fig. 1. As illustrated in Fig.1, titanium slag was mainly composed by anosovite phase ($M_xTi_{3-x}O_5$, $0 \leq x \leq 2$, M= Fe^{2+}, Mg^{2+}, etc.); while the phase of gangue minerals were not detected, which may be attributed to the too low concentration or the phase of gangue minerals with the nanocrystalline phases.

2.2 Characterization

The chemical compositions of raw titanium slag, the roasted slag and the final product were determined by X-ray fluorescence spectrometry (XRF, Shimadzu XRF-1800, Japan). The phase structures of raw titanium slag, the roasted slag and the final product were analyzed using the powder X-ray diffraction (Rigaku D/Max 2200 X, Japan), with a CuKα radiation source (λ=1.5418Å) and graphite monochromatic for the diffracted beam. The micro-morphological characteristics of raw titanium slag and the final product were characterized using a scanning electron microscope (XL30ESEM-TMP, Philips, Holland), operated at 20 kV in a low vacuum. The chemical bonds and structural functional groups of samples were performed by Raman spectrum with a confocal microprobe Raman system (Renishaw Raman Scope System 1000, UK).

2.3 Procedure

Na_2CO_3 decomposition method was proposed for producing rutile TiO_2 and simultaneously recover Cr(Ⅲ) and V(V) impurities from titanium slag, using the combined roasting-leaching process. Firstly, titanium slag and Na_2CO_3 agent were mixed with a desired mass ratio in a porcelain crucible. After fully mixing, 10.0 g of the mixture was introduced into a furnace to be roasted at an expected roasting temperature and roasting time. After roasting, the roasted slag was leached at 323.15 K using dilute sulfuric acid at a pH value of 2, with the liquid/solid (L/S) mass ratio of 10:1 for 1 h, to recovery Cr(Ⅲ) and V(V) impurities and accompany with a certain amount of Fe and Mg removed. Followed by the leached slag was treated through water wash, and then the washed sample was leached using 30 % sulfuric acid with the pulp ratio (S/L) of 1:5 for 6 h. Finally, the intermediate product was dried and then calcined under different conditions, and the subsequent characterizations of microcrystalline phase change of titanium slag were determined.

2.4 Thermodynamic calculation

Fig. 2 illustrated the relationship between the standard Gibbs free energy (ΔG^{θ}) with temperature for the sodium carbonate decomposition reactions probably occurred during the roasting process. Wherein the thermodynamics data was measured by FactSage and HSC thermodynamic software, between the temperature range of 300 K - 1400 K and at 1 atm standard state.

From the raw material analysis as shown in Table 1 and Fig. 1, it can be summarized that Panzhihua titanium slag had complicated compositions and structure, therefore the Gibbs free energy formations of the Na_2CO_3 decomposition reaction with titanium slag were calculated,

according to the thermodynamic characteristics of $MgTi_2O_5$, $FeTi_2O_5$, Al_2TiO_5, $MgTiO_3$, $FeTiO_3$ and TiO_2 phases, as detailed in reaction [1] to [7]. The Gibbs energy (ΔG^{θ}) plotted in Fig. 2 indicated that the reactions of sodium carbonate with titanium slag were feasible at temperatures higher than 1167.6 K, where the ΔG^{θ} values of reactions were negative. Furthermore, some silicate minerals in titanium slags also reacted with Na_2CO_3 at temperatures exceeding 1106.8 K, such as Mg_2SiO_4, Fe_2SiO_4, Al_2SiO_5 phases, as detailed in reaction [8] to [10]. The all involved reactions were presented as follows:

$$MgTi_2O_5(s) + 2Na_2CO_3(s) = 2Na_2TiO_3(s) + MgO(s) + 2CO_2(g) \quad [1]$$

$$FeTi_2O_5(s) + 2Na_2CO_3(s) = 2Na_2TiO_3(s) + FeO(s) + 2CO_2(g) \quad [2]$$

$$Al_2TiO_5(s) + 2Na_2CO_3(s) = Na_2TiO_3(s) + 2NaAlO_2(s) + 2CO_2(g) \quad [3]$$

$$MgTiO_3(s) + Na_2CO_3(s) = Na_2TiO_3(s) + MgO(s) + CO_2(g) \quad [4]$$

$$FeTiO_3(s) + Na_2CO_3(s) = Na_2TiO_3(s) + 2CO_2(g) \quad [5]$$

$$TiO_2(s) + 2Na_2CO_3(s) = Na_2TiO_3(s) + CO_2(g) \quad [6]$$

$$Fe_2O_3(s) + Na_2CO_3(s) = Na_2Fe_2O_4(s) + CO_2(g) \quad [7]$$

$$Mg_2SiO_4(s) + Na_2CO_3(s) = Na_2SiO_3(s) + 2MgO(s) + CO_2(g) \quad [8]$$

$$Fe_2SiO_4(s) + Na_2CO_3(s) = Na_2SiO_3(s) + 2FeO(s) + CO_2(g) \quad [9]$$

$$Al_2SiO_5(s) + 2Na_2CO_3(s) = Na_2SiO_3(s) + 2NaAlO_2(s) + 2CO_2(g) \quad [10]$$

3. Results and discussion

3.1 Proposed simultaneous recovery and preparation process

During the whole process, sodium roasting step renders an important influence on the removal of hazardous impurities and the upgrade of rutile TiO_2. Fang et al. and Liu et al.

proposed sodium slat roasting process to extract chromium (Cr) and vanadium (V) strongly embedded in vanadium slag, wherein chromium and vanadium was converted to water-soluble Na_2CrO_4 and Na_3VO_4 in short reaction time, then the reaction slurry was leached by dilute sulfuric acid, followed by the separation of chromium (Cr) and vanadium (V) was achieved by cooling and evaporation crystallization (Fang et al., 2012; Liu et al., 2013). Therefore, based on the above studies, the combined process for recovering chromium (Cr) and vanadium (V) and simultaneously upgrading rutile TiO_2 from titanium slag was proposed, as summarized in Fig. 3.

Firstly, raw titanium slag was subjected to roasting, where titanium in slag was converted to titanates. Meanwhile, chromium (Cr) and vanadium (V) was converted to soluble substances. Followed by the roasted slag was leached at 323.15 K using dilute sulfuric acid at a pH value of 2 and a liquid/solid (L/S) mass ratio of 10:1 for 1 h. After filtration, in the one hand, chromium (Cr) and vanadium (V) impurities in the leaching solution could be extracted by chemical methods, including solvent extraction, ion exchange or neutralization process; in the other hand, the residue was subjected to be leached using 30 % sulfuric acid with the pulp ratio (S/L) of 1:5 for 6 h. Wherein the titanium in roasted slag existed in the form of titanates, which could be dissolved in dilute sulphuric acid; meanwhile, other impurities such as Fe, Mg and Ca can also be dissolved in the acid condition. With the decrease of the sulphuric acid concentration, the titanium hydrolyzed from solution as anatase TiO_2, and the impurities still dissolved in solution. Furthermore, sulphuric acid can be recycled from the hydrolysis solution through a regeneration process. The impurities such as Fe, Mg and Ca can be separated by chemical precipitation, ion exchange method or adsorption method. After

leaching-hydrolysis-filtration treatment, the residue was through calcination treatment to obtain the final product, referring to rutile TiO_2.

3.2 Quality index analysis

To explore the optimal reaction conditions for removing hazardous Cr(Ⅲ) and V(V) impurities and simultaneously preparing high-grade rutile TiO_2, influence of experimental parameters on the quality index of rutile TiO_2 and the removal degree of Cr(Ⅲ) and V(V) impurities was systematically explored, including Na_2CO_3/slag mass ratio, roasting temperature and roasting time, and the results were presented in Fig. 4. Wherein the reaction process of Cr(Ⅲ) and V(V) were defined as the following equations,

$$Cr_2O_3(s) + Na_2CO_3(s) = 2Na_2Cr_2O_4(s) + CO_2(g) \quad [11]$$

$$V_2O_5(s) + Na_2CO_3(s) = NaVO_3(s) + CO_2(g) \quad [12]$$

3.2.1 Effects of the Na_2CO_3/slag mass ratio

Effects of Na_2CO_3/slag mass ratio were plotted in Fig. 4(a). As observed from Fig. 4(a), the improvement of Na_2CO_3/slag mass ratio contributed to the upgrade of rutile TiO_2 and reducing the vanadium and chromium contents in the roasted materials. Wherein as Na_2CO_3/slag mass ratio increased from 0.25 to 0.75, vanadium content sharply decreased from 2.32 % to 0.16 %. Additionally, for chromium content, it decreased from 0.83 % to 0.12 % with Na_2CO_3/slag mass ratio increased to 0.55; higher than 0.55, the change of chromium content was slight, with 0.11% at the Na_2CO_3/slag mass ratio increased to 0.75, showing an overall downward trend. From the above analysis, increasing Na_2CO_3 addition rendered a significant decrease of vanadium and chromium content; and based on the above results obtained from Fig. 4, it can be highlighted that sodium carbonate decomposition treatment

showed an effective and efficient effect to the recovery of V and Cr from titanium slag. Moreover, the TiO_2 grade increased from 70.12% to 81.92 % with Na_2CO_3/slag mass ratio increasing from 0.25 to 0.65, indicating that increasing Na_2CO_3 addition contributed to the upgraded transformation of Panzhihua titanium slag.

3.2.2 Effects of roasting temperature

Effects of roasting temperature were illustrated in Fig. 4(b). As seen from Fig. 4(b), the effects of roasting temperature were almost the same as that of Na_2CO_3/slag mass ratio. With roasting temperature increasing from 973.15 K to 1223.15 K, vanadium and chromium contents decreased from 0.32 % and 0.31 % to 0.03 % and 0.02 %, respectively, indicating that the increase of roasting temperature was beneficial to the removal of vanadium and chromium impurities. Moreover, it was observed that at temperature lower than 1173.15 K, the effects of roasting temperature on vanadium and chromium contents were significant; while temperature higher than 1173.15 K, the decrease of vanadium and chromium contents was obviously slight, which the change was ascribed to the limiting extent of titanium slag-sodium carbonate reaction occurred at temperatures lower than 1073.15 K, wherein presence of $MgTi_2O_5$ in the roasted sample hampered the removal of impurities during the subsequent leaching process. For TiO_2 grade, as shown in Fig. 4(b), the TiO_2 grade increased with the improvement of roasting temperature, with a maximum grade of 85.56 % at temperature improved to 1173.15 K; at temperatures exceeding 1173.15 K, the TiO_2 grade decreased marginally, which the decrease of the TiO_2 grade can be attributed to that the partial melting at high temperature caused a decrease in the material porosity, thereby affecting the leaching efficiency. The values change of vanadium and chromium contents and TiO_2 grade

with temperature suggested the optimum roasting temperature was reasonably considered to be 1173.15 K.

3.2.3 Effects of roasting time

Effects of roasting time were illustrated in Fig. 4(c). Observed from Fig. 4(c), the influence trend of roasting time was the same as that of Na_2CO_3/slag mass ratio and roasting temperature. As roasting time improved from 30 min to 120 min, vanadium and chromium contents decreased from 0.13 % and 0.11 % to 0.04 % and 0.03 %, respectively; while higher than 120 min, the decrease of vanadium and chromium contents was slight, with 0.036% and 0.038% at 150 min and 0.041% and 0.03% at 180 min, respectively. Therefore, the optimal roasting time could be concluded at 120 min, for the removal of vanadium and chromium contents in the roasted materials. In addition, as illustrated in Fig. 4(c), TiO_2 grade increased from 83.2 % to 85.56 % with roasting time increased to 120 min; while at a higher roasting time, TiO_2 grade decreased marginally, suggesting the optimum roasting time could be considered to be 120 min. The decrease of TiO_2 grade can be attributed to the increase of roasting time caused the formation of more refractories, which are less porous, further to hamper the leaching process and render the decrease of TiO_2 grade.

3.2.4 Chemical compositions analysis

Experiments were repeated under the optimized conditions, and the chemical compositions of the roasted slag and the final product were determined to analysis the merits of the proposed process, and the analytical results were presented in Table 2 and Table 3, respectively.

Table 2 displayed the chemical compositions of the roasted slag, with comparing the

chemical compositions of raw titanium slag (Table 1). Compared with Table 1 and Table 2, it can be concluded that after the sodium carbonate decomposition process, the composition contents of roasted slag slightly decreased. For the final product, as displayed in Table 3, the TiO_2 grade was 85.56 %, and the mineral contents decreased significantly compared with raw titanium slag and the roasted slag, including Mg, Al and Fe. Moreover, the contents of hazardous Cr_2O_3 and V_2O_5 impurities decreased sharply, declaring the highly efficient removal of Cr_2O_3 and V_2O_5 impurities from titanium slag.

Jarish proposed a process of recovery V and Cr and preparation synthetic TiO_2 by soda ash roasting-H_2SO_4 leaching process, wherein V and Cr were recovered through wet milling and filtration after roasting, with a two-step H_2SO_4 leaching process to remove impurities (Jarish, 1997). However, in the present work, only one-step acid leaching procedure was utilized, which was more economical and cost-efficient. Based on the above analysis, it could be concluded that during the upgrading process of rutile TiO_2, some elements were recovered and the sulfuric acid was recycled. Meanwhile, the residue generated from the leaching step contained trace amounts of hazardous elements such as Cr and V, while the hazardous elements were removed and the residue can safely dump in landfills after this proposed process. Moreover, the cost produced by this process will be reduced by recycling sulfuric acid. Thus, the proposed process was feasible with a good prospect for practical application.

3.3 Phase composition analysis

Effects of experimental parameters on the phase composition change of the roasted slag and the final product were comparatively investigated by XRD, including Na_2CO_3/slag mass ratio, roasting temperature and roasting time, and the results were plotted in Fig. 5.

3.3.1 Effects of the Na_2CO_3/slag mass ratio

Fig. 5(a) and Fig. 5(b) illustrated the effects of Na_2CO_3/slag mass ratio on the roasted slag and the final product, respectively, assessed with mass ratios ranging from 0.2 to 0.65 and roasted at 1123.15 K for 2 h.

For the roasted slag, it can be observed from Fig. 5(a) that with Na_2CO_3/slag mass ratio fixed at 0.2, the major phases were $MgTi_2O_5$ and rutile TiO_2, accompanied with diffraction peak of the titanates. The phase composition could be attributed to that the insufficient amount of Na_2CO_3 limited the reaction extent of raw material with sodium carbonate, further to hamper the transformation of titanates. As Na_2CO_3/slag mass ratio increased, the titanates were the main phases in the roasted slag, while the peaks of $MgTi_2O_5$ and rutile TiO_2 phases became weak. As Na_2CO_3/slag mass ratio increased to 0.6, the intensity of the titanates phase became stronger, and the peaks of $MgTi_2O_5$ and rutile TiO_2 disappeared, evidencing the completion of sodium carbonate decomposition reaction. For the final product, as observed from Fig. 5(b), the peak intensities of rutile TiO_2 phase increased distinctly with Na_2CO_3/slag mass ratio, while the tiny diffraction peak of $MgTi_2O_5$ was observed at lower Na_2CO_3/slag mass ratio, and disappeared at Na_2CO_3/slag mass ratio of 0.6. Therefore, the rutile TiO_2 with good crystalline rutile could be prepared at Na_2CO_3/slag mass ratio of 0.6.

3.3.2 Effects of roasting temperature

Fig. 5(c) and Fig. 5(d) presented effects of roasting temperature on the roasted slag and final product, respectively, covering a temperature range of 1023.15 K-1223.15 K and at a Na_2CO_3/slag mass ratio of 0.65, roasted with a duration time of 2 h.

Observed from Fig. 5(c), the major phases of the roasted slag were $MgTi_2O_5$ and Na_2CO_3,

accompanied with the presence of rutile and titanates at 1123.15 K. The low presence of rutile and titanates was attributed to the reaction extent of raw material with sodium carbonate was low at low temperature, hence rendering the transformation of titanates incomplete., which the result was consistent with the Gibbs analysis. With the increase in temperature, the main phase of the roasted slag was transformed into titanates and the peaks of rutile disappeared, indicating the reaction extent of titanium slag-sodium carbonate improved at temperatures higher than 1123.15 K. As seen from Fig. 5(d), the peak intensities of rutile TiO_2 phase increased distinctly with roasting temperature continuously improved to1173.15 K; while higher than 1173.15 K, the peak intensities of rutile TiO_2 phase decreased marginally.

3.3.3 Effects of roasting time

Fig. 5(e) and (f) displayed effects of roasting time on the roasted slag and the final product, respectively, covering a roasting time regime from 30 min to 180 min, and assessed at a Na_2CO_3/slag mass ratio of 0.65 and roasted at a roasting temperature of 1173.15 K.

From Fig. 5(e), the major phases of the roasted slag were titanates at roasting time of 30 min. Notably, the titanates phase had insignificant change with roasting time increased from 30 min to 150 min, just with the phenomenon occurred that the intensities of phases obviously increased with roasting time, indicating that roasting time rendered an insignificant effect on the sodium carbonate decomposition reaction. From Fig. 5(f), for the final product, the results indicated that the peak intensities of rutile TiO_2 phase distinctly improved with roasting time, while decreased marginally in the time interval from 120 min to 150 min. Meanwhile, the transformation of titanium slag to rutile TiO_2 could be confirmed to attain the maximum value with 120 min of roasting time treatment.

3.4 Microstructure characterization

Effects of calcination duration and calcination temperature on the micro-morphological characteristics of the final product were analyzed by SEM, and the results were illustrated in Fig. 6.

Fig. 6(a)-(c) illustrated the effects of calcination duration at a calcination temperature of 1123.15 K, with calcination durations of 30 min, 90 min and 150 min. From Fig. 6(a), it can be seen that at a calcination duration of 30 min, the sample was heterogeneous with consisting of small irregular particles. With the increase in roasting time, the diameter of particles did not increase apparently, indicating that the influence of roasting time on the morphology change of rutile TiO_2 was insignificant. In addition, Fig. 6(d)-(f) displayed the influence of calcination temperature with a calcination duration of 120 min, with calcination temperature covering 1233.15 K, 1273.15 K, and 1323.15 K. It was observed that with calcination temperature increased from 1233.15 K to 1273.15 K, the particles coarsen and numerous short rod-like particles appeared. At a roasting temperature of 1323.15 K, some particles were fused, which was ascribed to the sintering of adjacent particles. Therefore, it can be concluded that calcination temperature presented a positive effect on the microstructure morphology change of rutile TiO_2. Moreover, it can be observed from Fig. 6(d)-(f) that the crystal of rutile TiO_2 presented the anisotropy with a preferential growth, imposing a short rod-like shape. With the comparison between the influence of calcination duration and calcination temperature on the micro-morphological characteristics of the final product, it can be concluded that calcination temperature was the main physical parameter driving such anisotropy in the short rod-like shape (Sathyaseelan et al., 2016).

3.5 Phase composition and morphology change analysis

During the proposed process, raw titanium slag was roasted with Na_2CO_3 additive; followed by the roasted slag was washed with water and then hydrolyzed with 30 % boiling sulfuric acid; finally, the final product, the rutile TiO_2 was produced by calcining the leaching residue. The product produced from different reaction stages corresponded to different phase composition and morphology. Therefore, to determine effects of different process on the phase composition and morphology change of the product at different stages during the roasting-leaching process were investigated by XRD, Raman spectroscopy, and SEM-EDAX characterization, respectively, and the results were presented in Fig. 7, Fig. 8 and Fig. 9, respectively.

3.5.1 XRD characterization

Fig. 7(a) displayed the XRD patterns of titanium slag at different reaction stages. For the raw titanium slag, it was observed that $M_xTi_{3-x}O_5$ ($0 \leq x \leq 2$) phase was the major phase. After the soda ash roasting treatment, Na-Mg-Ti-O phase in the roasted slag was detected with clear formation, attributed to the presence of Na_2CO_3 additive, with the other peaks corresponded to $Na_2Ti_6O_{13}$ phase. This result was slightly different from Lasheen's report (Lasheen et al., 2008), which applied the same method to treat titanium slag. The difference of results obtained by the same method can be attributed to the difference of two feedstocks and the complexity of Panzhihua titanium slag as well; additionally, the insufficient addition of sodium carbonate may contribute to limiting the extent of reaction. Moreover, by comparing the raw slag and the calcined slag, the strong preferential orientation of (110) and (101) planes of the calcined slags were detected, wherein the strongest peaks of rutile TiO_2 phase (JCPD

card NO.21-1276) occurred at 2θ=27.44°and 2θ=36.07°, the third strongest peak was appeared at 2θ=54.32°, which belonged to the orientation (211) peak, indicating that rutile TiO_2 with high crystallinity was produced.

3.5.2 Raman spectroscopy characterization

Fig. 7(b) illustrated the Raman spectra of titanium slag at different reaction stages. For the raw titanium slag, as shown in Fig. 7(b), the Raman modes appeared at 170.2 cm^{-1}, 430.5 cm^{-1}, and 616.4 cm^{-1}. Wherein the Oscillating vibration of O-Ti-O bond of Ti_3O_5 caused the Raman modes at 170.2 cm^{-1} (Chen et al., 2014a); the twisting vibration of O-Ti-O of the rutile TiO_2 caused the characteristic Raman band of rutile TiO_2 detected at 430.5 cm^{-1} (Chen et al., 2013b); in addition, the symmetric stretching vibrations of anatase TiO_2 caused the Raman band observed at 616.4 cm^{-1} (Chen et al., 2014a). For the acid leached slag, as illustrated in Fig. 7(b), the four bands of the anatase TiO_2 crystalline phase were observed to appear at 156.7 cm^{-1}, 398.4 cm^{-1}, 508.2 cm^{-1}, and 618.1 cm^{-1}, corresponding to the Raman active modes including E_g (156.7, 616.4), B_{1g} (398.4) and A_{1g} (508.2) (Guéguin et al., 2007). Based on the above results, it could be concluded that the phases formed in the roasting step were dissolved by sulphate acid, representing that the anatase TiO_2 was the precipitate from hydrolyzing the titanium. Furthermore, the impurities associated with the roasted product were transformed into soluble substances, including Fe, Mg, Ca, and Al, etc. Similarly, as observed from Fig. 7(b), for the slag calcined at 1223.15 K for 60 min, the calcined sample had two strong peaks at 442.3 cm^{-1} and 609.7 cm^{-1}, and the three peaks with moderate intensity were observed at 141.5 cm^{-1}, 237.8 cm^{-1} and 785.3 cm^{-1}, respectively, which belonged to rutile TiO_2 Raman active modes (Wu et al., 2012; Xiao et al., 2007; You et al., 2004), indicating the formation of

rutile TiO_2. The results proved that the anatase TiO_2 was transformed into rutile TiO_2 at 1223.15 K, representing by the characteristic Raman peaks of anatase TiO_2 disappeared. Moreover, the Raman spectroscopy results were consistent with the results of XRD analysis.

3.5.3 SEM-EDAX characterization

Scanning electron microscope (SEM) and EDAX attached to SEM were utilized to determine the microstructures of titanium slag before and after the proposed process treatment, and the rustles were presented in Fig. 8 and Fig. 9, respectively.

Fig. 8 illustrated the microstructure morphology of the raw titanium slag and the final product. As observed from Fig. 8(a)-(b), the surfaces of the raw titanium slag were smooth without visible pits or cracks. As observed from Fig. 8(c)-(d), compared with the morphology of the final product, referring to the calcined slag, the rutile TiO_2 crystals were formed on the surface of the calcined slag. Moreover, rutile TiO_2 with the rod-like structure was characterized by accompanied with the relatively loose morphology. The morphology transformation of raw titanium slag as massive grains to the rod-like structure was attributed to the formation of rutile TiO_2.

Fig. 9 showed the EDAX spectra and SEM image of the final product. EDAX analysis indicated that the sample consisted of Ti-oxide and a phase mainly composed by Si and S element, additionally accompanying with a minor amount of Fe and Mg elements; however, these phases without detected by XRD, which could be attributed to that these phases were nanocrystalline substances or the too-low concentrations of those phases. The results indicated that impurities in the final product had been mostly removed by the distilled water and sulphuric acid leaching, and the results were consistent with Table 3.

Additionally, Cr_2O_3 and V_2O_5 material have been reported to be widely applied in the engineering of various smart and multifunctional nanomaterials and devices (Kana, et al., 2010; Khamlich, et al., 2011a; Khamlich, et al., 2011b; Simo, et al., 2014; Sone, et al., 2012). In the presented work, the Cr_2O_3 and V_2O_5 as hazardous impurities was efficiently removed and recovered from ilmenite slag via sodium carbonate decomposition process, simultaneously producing high-quality rutile TiO_2, greatly achieving the value-added effect and clean utilization of titanium slag. To further improve upon the quality indexes of rutile TiO_2 and the removal degree of Cr_2O_3 and V_2O_5 impurities in titanium slag, a study on the optimization of parameters in acid leaching experiment was currently being conducted.

4. Conclusions

In the work, simultaneously recovering hazardous Cr(Ⅲ) and V(V) impurities and producing high-grade rutile TiO_2 from titanium slag was attempted using sodium carbonate roasting. The roasting conditions for formation sodium titanates were optimized with Na_2CO_3 to slag mass ratio of 0.65:1 at 1173.15 K for 120 min. Vanadium and chromium can be efficiently recovered by leaching the roasted slag with dilute sulfuric acid, with the contents decreased to 0.03 % and 0.04 %, respectively; meanwhile, rutile TiO_2 was successfully synthesized by the leaching residue calcined at 1323.15 K with duration of 120 min, with a high grade of 85.56%. XRF and EDAX results indicated that Cr(Ⅲ) and V(V) impurities and Mg, Al and Fe oxides were removed by this proposed method, highlighting it is an effective way of removing hazardous metals from titanium slag. Moreover, XRD results confirmed the transformation of titanium slag into rutile TiO_2, with high crystallinity, which was consistent

with SEM results and Raman spectroscopy analysis, with the peaks of rutile TiO_2 phase characterized at 175.3 cm^{-1}, 237.5 cm^{-1}, 442.3 cm^{-1}, 609.7 cm^{-1} and 785.3 cm^{-1}. The work confirms effective removal of Cr(Ⅲ) and V(V) and preparation of high-grade rutile TiO_2 by using sodium carbonate decomposition, furthermore demanding further studies to explore the economic feasibility for commercial adoption.

Author Contributions Section

Prof. Guo Chen, Prof. Jin Chen and Prof. Jinhui Peng conceived and designed the study. Miss Aoxi He, Miss Qi Jiang, Dr. Mamdouh Omran and Prof. Guo Chen performed the experiments. Prof. Jinhui Peng and Prof. Guo Chen provided the raw materials, and Prof. Jinhui Peng provided the box-type microwave high temperature furnace. Miss Aoxi He, Mr. Kangqiang Li and Prof. Jin Chen wrote the paper. Miss Aoxi He, Mr. Kangqiang Li, Dr. Mamdouh Omran and Prof. Guo Chen reviewed and edited the manuscript. All authors read and approved the manuscript.

Declaration of interests

☒ The authors declare that they have no known competing financial interests or personal relationships that could have appeared to influence the work reported in this paper.

Acknowledgements

The authors acknowledge the financial supports from the National Natural Science

Foundation of China (No: U1802255, 51504110 and 51424114), Yunnan Applied Basic Research Project of China (No: 2017FD117) and Innovative Research Team (in Science and Technology) in University of Yunnan Province were sincerely acknowledged.

References

[1] Chen, D.S., Zhao, L.S., Liu, Y.H., Qi, T., Wang, J.C., Wang, L.N., 2013. A novel process for recovery of iron, titanium, and vanadium from titanomagnetite concentrates: NaOH molten salt roasting and water leaching processes. J. Hazard. Mater. 244, 588-595. https://doi.org/10.1016/j.jhazmat.2012.10.052.

[2] Chen, G., Chen, J., Song, Z.K., Srinivasakannan, C., Peng, J.H., 2014. A new highly efficient method for the synthesis of rutile TiO_2. J. Alloy. Compd. 585(1), 5-77. https://doi.org/10.1016/j.jallcom.2013.09.056.

[3] Chen, G., Song, Z.K., Chen, J., Srinivasakannan, C., Peng, J.H., 2013. Investigation on phase transformation of titania slag using microwave irradiation. J. Alloy. Compd. 579(31), 612-616. https://doi.org/10.1016/j.jallcom.2013.07.112.

[4] Chen, G., Xiong, K., Peng, J.H., Chen, J., 2010. Optimization of combined mechanical activation-roasting parameters of titania slag using response surface methodology. Adv. Powder. Technol. 21(3), 331-335. https://doi.org/10.1016/j.apt.2009.12.017.

[5] Dong, H.G., Jiang, T., Guo, Y.F., Chen, J.L., Fan, X.X., 2012. Upgrading a Ti-slag by a roast-leach process. Hydrometallurgy. 113, 119-121. https://doi.org/10.1016/j.hydromet.2011.12.008.

[6] Eriksson, G., Pelton, A.D., Woermann, E., Ender, A., 1996. Measurement and thermodynamic evaluation of phase equilibrium in the Fe-Ti-O system. Berichte. Der. Bunsen-Ges. Phys. Chem. 100(11), 1839-1849. https://doi.org/10.1002/bbpc.19961001114.

[7] Fang, H.X., Li, H.Y., Xie, B., 2012. Effective chromium extraction from chromium-containing vanadium slag by sodium roasting and water leaching. Iron. Steel. Inst. Japan. Intern. 52(11), 1958-1965. https://doi.org/10.2355/isijinternational.52.1958.

[8] Grätzel, M., 2003. Dye-sensitized solar cells. J. Photoch. Photobio. C. 4(2), 145-153. https://doi.org/10.1016/S1389-5567(03)00026-1.

[9] Guéguin, M., Cardarelli, F., 2007. Chemistry and mineralogy of titania-rich slags. part 1 hemo-ilmenite, sulphate, and upgrade titania slags. Min. Proc. Ext. Metall. Rev. 28(1), 1-58. https://doi.org/10.1080/08827500600564242.

[10] Guo, Y.F., Liu, S.S., Jiang, T., Qiu, G.Z., Chen, F., 2014. A process for producing synthetic rutile from Panzhihua titanium slag. Hydrometallurgy. 147(8), 134-141. https://doi.org/10.1016/j.hydromet.2014.05.009.

[11] Hearne, G.R., Zhao, J., Dawe, A.M., Pischedda, V., Maaza, M., Nieuwoudt, M.K., Pierre Kibasomba, P., Nemraoui, O., 2004. Effect of grain size on structural transitions in anatase TiO_2: A Raman spectroscopy study at high pressure. Phys. Rev. B. 70(13), 134102. https://doi.org/10.1103/PhysRevB.70.134102.

[12] Huang, R., Lv, X.W., Bai, C.G., Zhang, K., 2013. Enhancement reduction of Panzhihua ilmenite concentrate with coke and conglomeration of metal with ferrosilicon. Steel. Res. Int. 84(9), 892-899. https://doi.org/ 10.1002/srin.201200330.

[13] Huang, R., Lv, X.W., Bai, C.G., Deng, Q.Y., 2012. Solid state and smelting reduction of Panzhihua ilmenite concentrate with coke. Can. Metall. Quart. 51(4), 434-439. https://doi.org/ 10.1179/1879139512Y.0000000008.

[14] Jarish, B., Upgrading Sorel slag for production of synthetic rutile: U.S. Patent 4, 038, 363. 1977-7-26.

[15] Kana, J.B.K., Ndjaka, J.M., Ngom, B.D., Manyala, N., Nemraoui, O., Fasasi, A.Y., Nemutudi, R., Gibaud, A., Knoesen, D., Maaza, M., 2010. Thermochromic nanocrystalline Au-VO_2 composite thin films prepared by radiofrequency inverted cylindrical magnetron sputtering. Thin. Solid. Films. 518 (6), 1641-1647. https://doi.org/10.1016/j.tsf.2009.11.074.

[16] Kaviyarasu, K., Geetha, N., Kanimozhi, K., Maria Magdalane, C., Sivaranjani, S., Ayeshamariam, A., Kennedy, J., Maaza, M., 2017. In vitro cytotoxicity effect and antibacterial performance of human lung epithelial cells A549 activity of Zinc oxide doped TiO_2 nanocrystals: Investigation of bio-medical application by chemical method. Mater. Sci. Eng. C. 74, 325-333. https://doi.org/10.1016/j.msec.2016.12.024.

[17] Kaviyarasu, K., Kennedy, J., Manikandan, E., Mohamed, H., Maaza, M., 2016. Photodegradation of organic pollutants RhB dye using UV simulated sunlight on ceria ba sed TiO_2 nanomaterials for antibacterial applications. Sci. Rep-UK. 6, 38064. https://doi.org/10.1038/srep38064.

[18] Khamlich, S., Manikandan, E., Ngom, B.D., Sithole, J., Nemraoui, O., Zorkani, I., McCrindle, R., Cingo, N., Maaza, M., 2011a. Synthesis, characterization, and growth

mechanism of α-Cr_2O_3 monodispersed particles. J. Phys. Chem. Solids. 72(6), 714-718. https://doi.org/10.1016/j.jpcs.2011.02.015.

[19] Khamlich, S., Srinivasu, V.V., Nemraoui, O., McCrindle, R., Cingo, N., Maaza, M., 2011b. Electron spin resonance study of α-Cr_2O_3 and Cr_2O_3• nH_2O quasi-spherical nanoparticles. Nanosci. Nanotech. Let. 3(4), 550-555. https://doi.org/10.1166/nnl.2011.1217.

[20] Lasheen, T.A., 2008. Soda ash roasting of titania slag product from Rosetta ilmenite. Hydrometallurgy. 93(3-4), 124-128. https://doi.org/10.1016/j.hydromet.2008.02.020.

[21] Li, K.Q., Chen, J., Chen, G., Peng,, J.H., Ruan, R., Srinivasakannan, C., 2019a. Microwave dielectric properties and thermochemical characteristics of the mixtures of walnut shell and manganese ore. Bioresource. Technol. 286, 121381. https://doi.org/10.1016/j.biortech.2019.121381.

[22] Li, K.Q., Chen, G., Chen, J., Peng, J.H., Ruan, R., Srinivasakannan, C., 2019b. Microwave pyrolysis of walnut shell for reduction process of low-grade pyrolusite. Bioresource. Technol. 291, 121838. https://doi.org/10.1016/j.biortech.2019.121838.

[23] Li, K.Q., Chen, G., Li, X.T., Peng, J.H., Ruan, R., Omran, M., Chen, J., 2019c. High-temperature dielectric properties and pyrolysis reduction characteristics of different biomass-pyrolusite mixtures in microwave field. Bioresource. Technol. 294, 122217. https://doi.org/10.1016/j.biortech.2019.122217.

[24] Li, K.Q., Chen, J., Peng, J.H., Koppala, S., Omran, M., Chen, G., 2020a. One-step preparation of CaO-doped partially stabilized zirconia from fused zirconia. Ceram. Int. https://doi.org/10.1016/j.ceramint.2019.11.129.

[25] Li, K.Q., Chen, J., Peng, J.H., Ruan, R., Srinivasakannan, C., Chen, G., 2020b. Pilot-scale study on enhanced carbothermal reduction of low-grade pyrolusite using microwave heating. Powder. Technol. 360, 846-854. https://doi.org/10.1016/j.powtec.2019.11.015.

[26] Li, K.Q., Jiang, Q., Chen, J., Peng, J.H., Li, X.P., Koppala, S., Omran, M., Chen, G., 2020c. The controlled preparation and stability mechanism of partially stabilized zirconia by microwave intensification. Ceram. Int. https://doi.org/10.1016/j.ceramint.2019.11.251.

[27] Li, K.Q., Chen, J., Peng, J.H., Ruan, R., Orman, M., Chen, G., 2020d. Dielectric properties and thermal behavior of electrolytic manganese anode mud in microwave field. J. Hazard. Mater. 381, 121227. https://doi.org/10.1016/j.jhazmat.2019.121227.

[28] Liu, B., Du, H., Wang, S.N., Zhang, Y., 2013. A novel method to extract vanadium and chromium from vanadium slag using molten NaOH-$NaNO_3$ binary system. AIChE. J. 59(2), 541-552. https://doi.org/10.1002/aic.13819.

[29] Liu, S.S., Guo, Y.F., Qiu, G.Z., Jiang, T., Chen, F., 2013. Preparation of Ti-rich material from titanium slag by activation roasting followed by acid leaching. T. Nonferr. Metal. Soc. 23(4), 1174-1178. T. Nonferr. Metal. Soc. https://doi.org/10.1016/S1003-6326(13)62580-7.

[30] Liu, Y.H., Meng, F.C., Fang, F.Q., Wang, W.J., Chu, J.L., Tao, Q., 2015. Preparation of rutile titanium dioxide pigment from low-grade titanium slag pretreated by the NaOH molten salt method. Dyes. Pigments. 125, 384-391. https://doi.org/10.1016/j.dyepig.2015.10.036.

[31] Nayl, A.A., Ismail, I.M., Aly, H.F., 2009. Ammonium hydroxide decomposition of ilmenite slag, Hydrometallurgy. 98(1), 196-200. https://doi.org/10.1016/j.hydromet.2009.04.011.

[32] Saha, R., Nandi, R., Saha, B., 2011. Sources and toxicity of hexavalent chromium. J. Coord. Chem. 64(10), 1782-1806. https://doi.org/10.1080/00958972.2011.583646.

[33] Saha, R., Saha, I., Nandi, R., Ghosh, A., Basu, A., Ghosh, S.K., Saha, B., 2013. Application of Chattim tree (Devil tree, Alstonia scholaris) saw dust as a biosorbent for removal of hexavalent chromium from aqueous solution. Can. J. Chem. Eng. 91(5), 814-821. https://doi.org/10.1002/cjce.21703.

[34] Samal, S., Mohapatra, B.K., Mukherjee, P.S., Chatterjeea, S.K., 2009. Integrated XRD, EPMA and XRF study of ilmenite and titania slag used in pigment production. J. Alloy. Compd. 474(1), 484-489. https://doi.org/10.1016/j.jallcom.2008.06.121.

[35] Sathyaseelan, B., Manikandan, E., Lakshmanan, V., Baskaran, I., Sivakumar, K., Ladchumananandasivam, R., Kennedy, J., Maaza, M., 2016. Structural, optical and morphological properties of post-growth calcined TiO_2 nanopowder for opto-electronic device application: Ex-situ studies. J. Alloy. Compd. 671, 486-492. https://doi.org/10.1016/j.jallcom.2016.02.105.

[36] Simo, A., Mwakikunga, B., Sone, B.T., Julies, B., Madjoe, R., Maaza, M., 2014. VO_2 nanostructures based chemiresistors for low power energy consumption hydrogen sensing. Int. J. Hydrogen. Energ. 39(15), 8147-8157. https://doi.org/10.1016/j.ijhydene.2014.03.037.

[37] Sone, B.T., Benoit, R., Zongo, S., Bucher, R., Maaza, M., 2012. Time-based investigation of the growth of VO_2 (B) micro and nanostructures on vanadium by hydrothermal synthesis. Mater. Chem. Phys. 136(2-3), 358-370. https://doi.org/10.1016/j.matchemphys.2012.06.041.

[38] Xiang, J.Y., Huang, Q.Y., Lv, X.W., Bai, C.G., 2017. Multistage utilization process for the gradient-recovery of V, Fe, and Ti from vanadium-bearing converter slag. J. Hazard. Mater. 336, 1-7. https://doi.org/10.1016/j.jhazmat.2017.04.060.

[39] Xiao, P., Zheng, S.B., You, J.L., Jiang, G.C., Chen, H., Zeng, H., 2007. Structure and Raman spectra of titanium oxides. Spectrosc. Spect. Anal. 27(5), 936-939. https://doi.org/10.3321/j.issn:1000-0593.2007.05.026.

[40] Wu, J.C., Ren, Y.P., Wang, B., 2012. Quantitative analysis of the content of rutile TiO_2 by Raman spectrum. Chin. J. Anal. Lab. 31(12), 100-103. https://doi.org/10.13595/j.cnki.issn1000-0720.2012.0359.

[41] Ye, Q.X., Ru, J.J., Peng, J.H., Chen, G., Wang, D., 2018. Formation of multiporous MnO/N-doped carbon configuration via carbonthermal reduction for superior electrochemical properties. Chem. Eng. J. 331, 570-577. https://doi.org/10.1016/j.cej.2017.09.031.

[42] You, J.L., Jiang, G.C., Wang, Z.S., Pan, X.Y., Ma, X.M., 2004. High temperature Raman spectroscopic study of titania and its phase transformation. Chin. J. Light. Scat. 16(2), 95-98. https://doi.org/10.3969/j.issn.1004-5929.2004.02.001.

[43] Zhang, S., Nicol, M.J., 2010. Kinetics of the dissolution of ilmenite in sulfuric acid solutions under reducing conditions. Hydrometallurgy. 103(1), 196-204. https://doi.org/10.1016/j.hydromet.2010.03.019.

[44] Zhao, L.S., Wang, L.N., Qi, T., Chen, D.S., Zhao, H.X., Liu, Y.H., 2014. A novel method to extract iron, titanium, vanadium, and chromium from high-chromium vanadium-bearing titanomagnetite concentrates. Hydrometallurgy. 149, 106-109. https://doi.org/10.1016/j.hydromet.2014.07.014.

Table captions

Table 1 Chemical compositions of Panzhihua titanium slag

Table 2 Chemical compositions of the roasted slag

Table 3 Chemical compositions of the final product

Figure captions

Fig. 1 XRD pattern of Panzhihua titanium slag

Fig. 2 Dependency of ΔG^{θ} on temperatures for sodium carbonate decomposition reactions of titanium slag

Fig. 3 Proposed processes for recovering vanadium (V) and chromium (Cr) and simultaneously preparing rutile TiO_2

Fig. 4 Effects of experimental parameters on TiO_2 grade and vanadium (V) and chromium (Cr) contents in the roasted materials, (a) Na_2CO_3/slag mass ratio; (b) roasting temperature; (c) roasting time

Fig. 5 XRD patterns of the roasted slag and the final product at different conditions, (a) the roasted slag with Na_2CO_3/slag mass ratio; (b) the final product with Na_2CO_3/slag mass ratio; (c) the roasted slag with roasting temperature; (d) the final product with roasting temperature; (e) the roasted slag with roasting time; (f) the final product with roasting time

Fig. 6 SEM patterns of the final product under different calcination conditions

Fig. 7 XRD patterns and Raman spectra of samples at different stages, (a) XRD patterns; (b) Raman spectra

Fig. 8 SEM images of raw titanium slag and the final product, (a) raw titanium slag, 3000×; (b) raw titanium slag, 6000×; (c) the final product, 8000×; (d) the final product, 16000×

Fig. 9 EDAX spectra and (a) SEM image of the final product, (b) district 1; (c) district 2; (d) spot 3

Table 1 Chemical compositions of Panzhihua titanium slag

Composition	TiO_2	Fe_2O_3	Al_2O_3	MgO	SiO_2	CaO	Cr_2O_3	V_2O_5
Mass/W%	71.82	8.92	3.69	7.32	2.63	1.78	0.86	2.64

Table 2 Chemical compositions of the roasted slag

Composition	TiO_2	Fe_2O_3	Al_2O_3	MgO	SiO_2	CaO	Cr_2O_3	V_2O_5
Mass/W%	69.72	7.13	2.54	5.64	1.28	1.15	0.73	2.32

Table 3 Chemical compositions of the final product

Composition	TiO_2	Fe_2O_3	Al_2O_3	MgO	SiO_2	CaO	Cr_2O_3	V_2O_5
Mass/W%	85.56	1.76	0.10	0.42	2.51	1.772	0.03	0.04

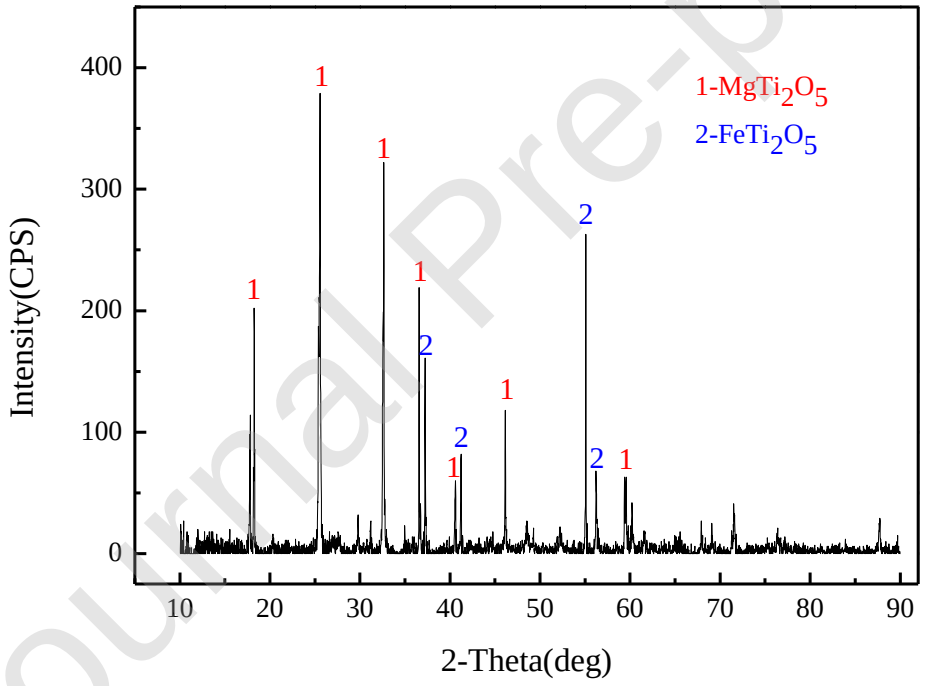

Fig. 1 XRD pattern of Panzhihua titanium slag.

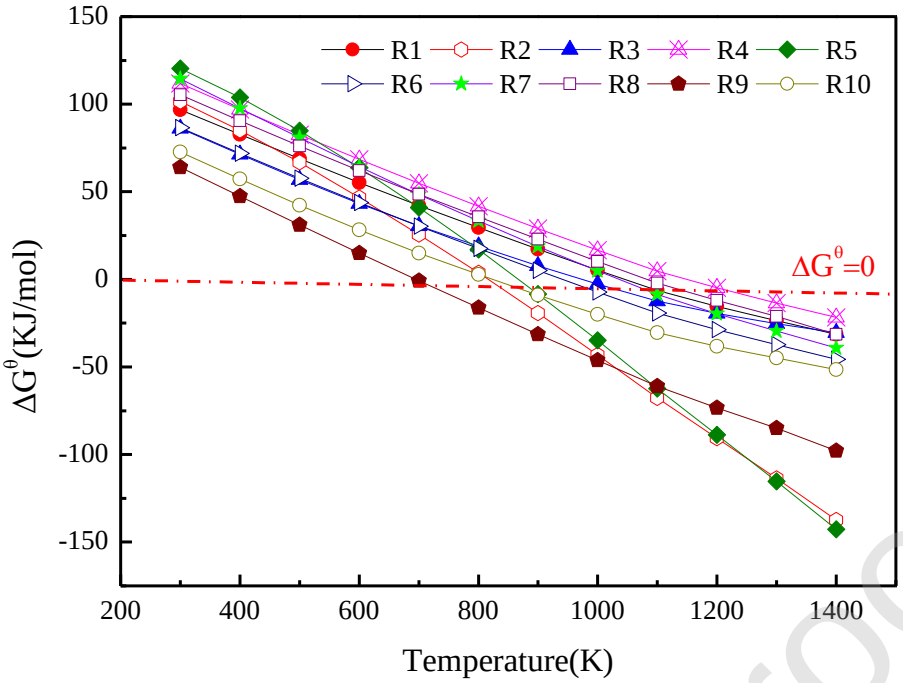

Fig. 2 Dependency of ΔG^{θ} on temperatures for sodium carbonate decomposition reactions of titanium slag. R* represents the reaction as listed.

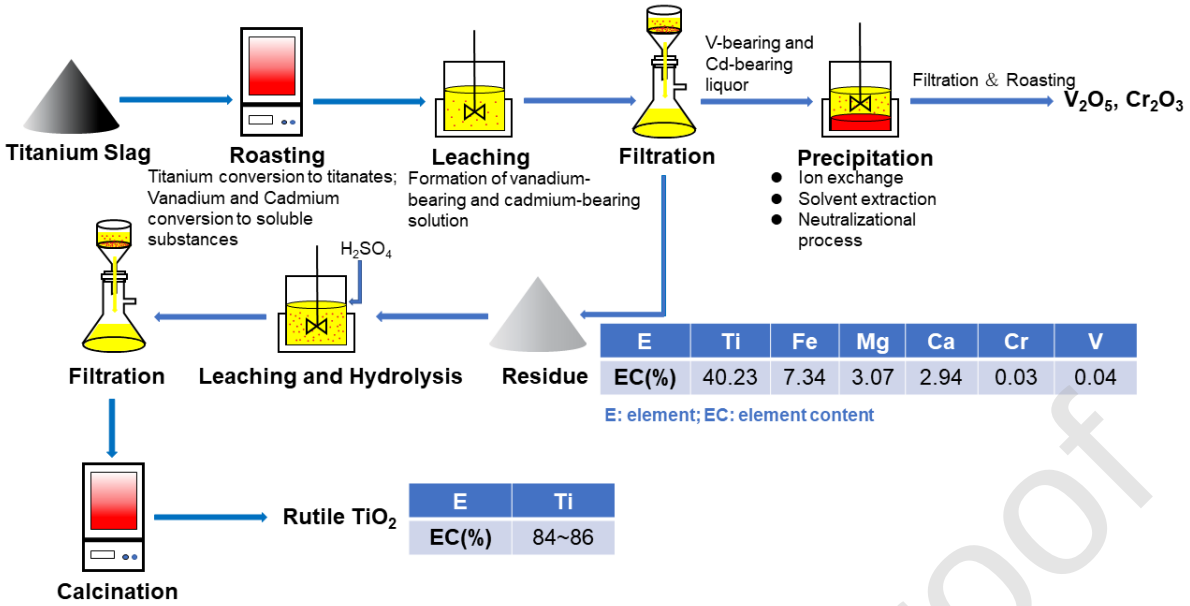

E	Ti	Fe	Mg	Ca	Cr	V
EC(%)	40.23	7.34	3.07	2.94	0.03	0.04

E: element; EC: element content

E	Ti
EC(%)	84~86

Fig. 3 Proposed processes for recovering vanadium (V) and chromium (Cr) and simultaneously preparing rutile TiO_2.

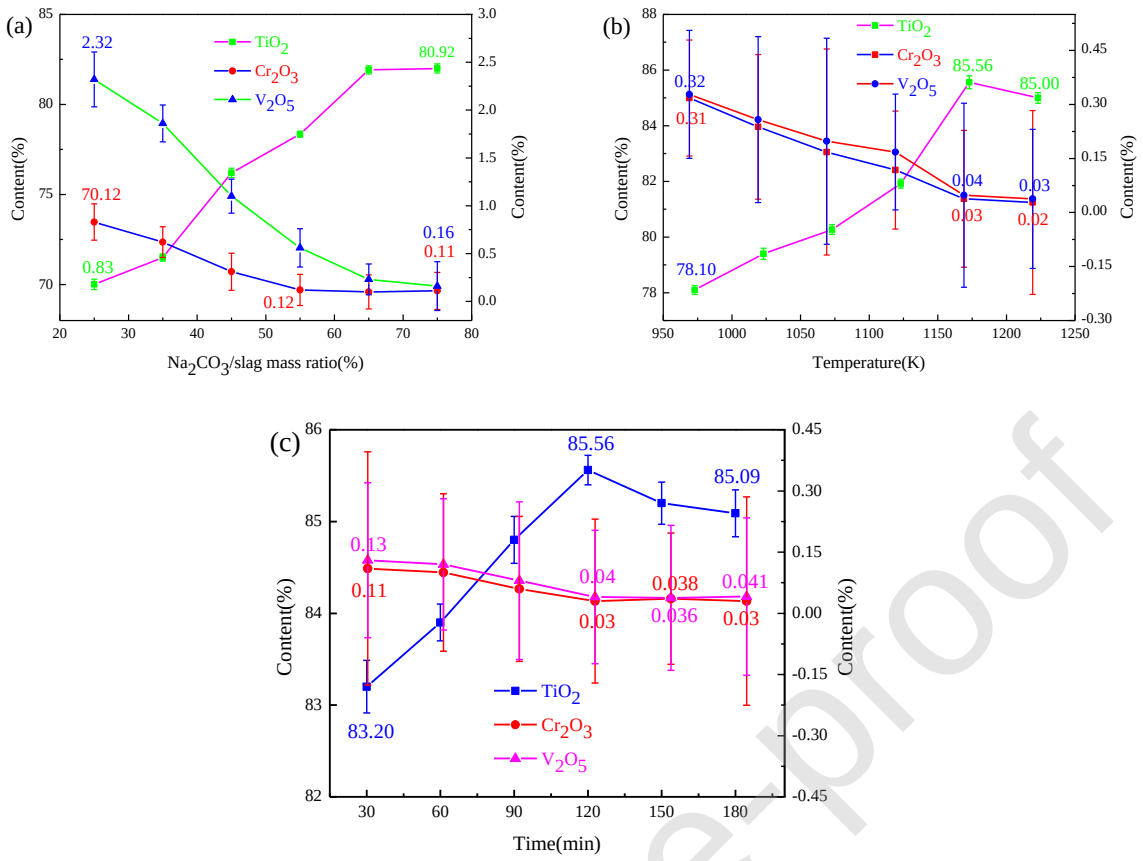

Fig. 4 Effects of experimental parameters on TiO_2 grade and vanadium (V) and chromium (Cr) contents in the roasted materials, (a) Na_2CO_3/slag mass ratio; (b) roasting temperature; (c) roasting time.

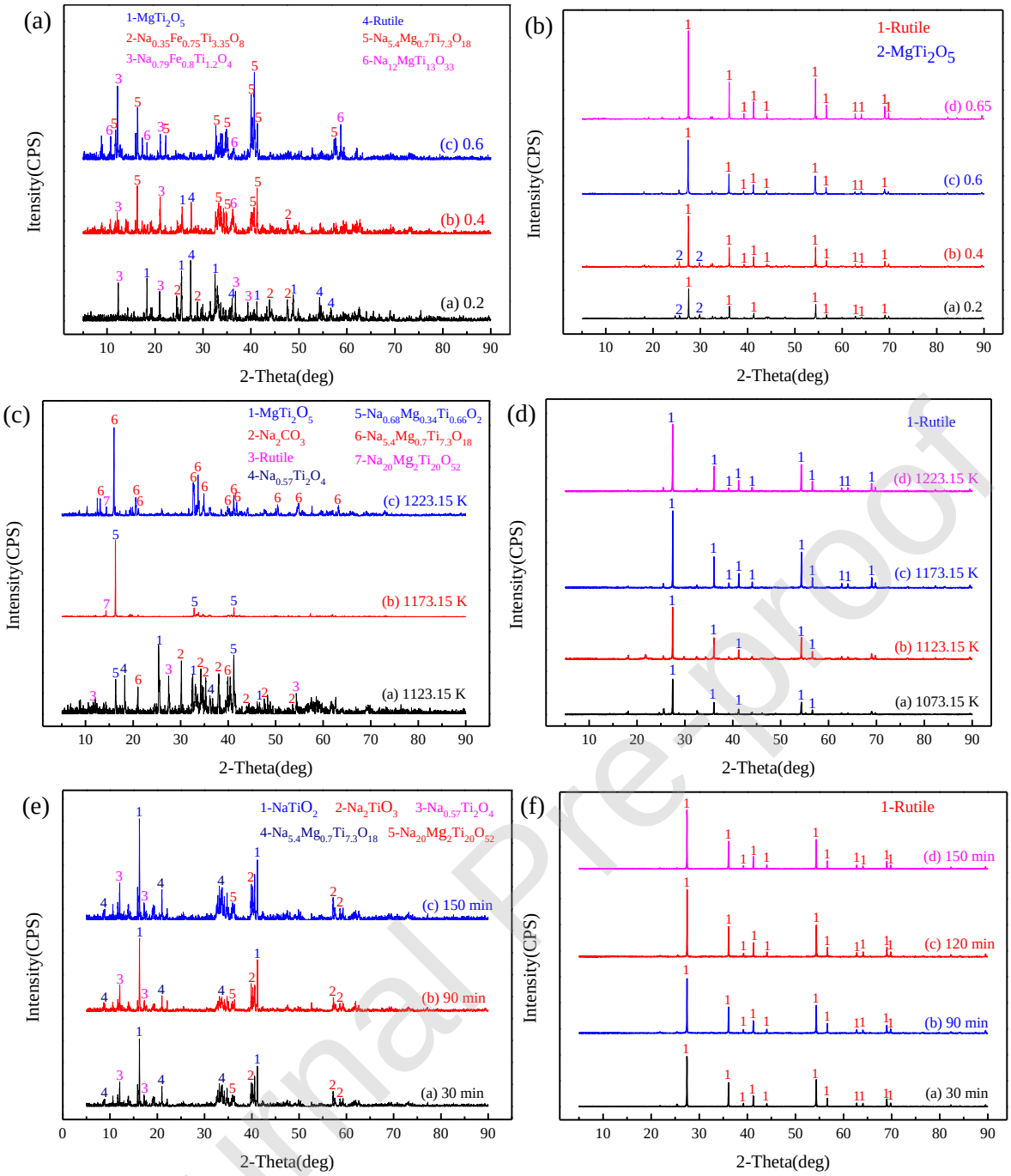

Fig. 5 XRD patterns of the roasted slag and the final product at different conditions, (a) the roasted slag with Na_2CO_3/slag mass ratio; (b) the final product with Na_2CO_3/slag mass ratio; (c) the roasted slag with roasting temperature; (d) the final product with roasting temperature; (e) the roasted slag with roasting time; (f) the final product with roasting time.

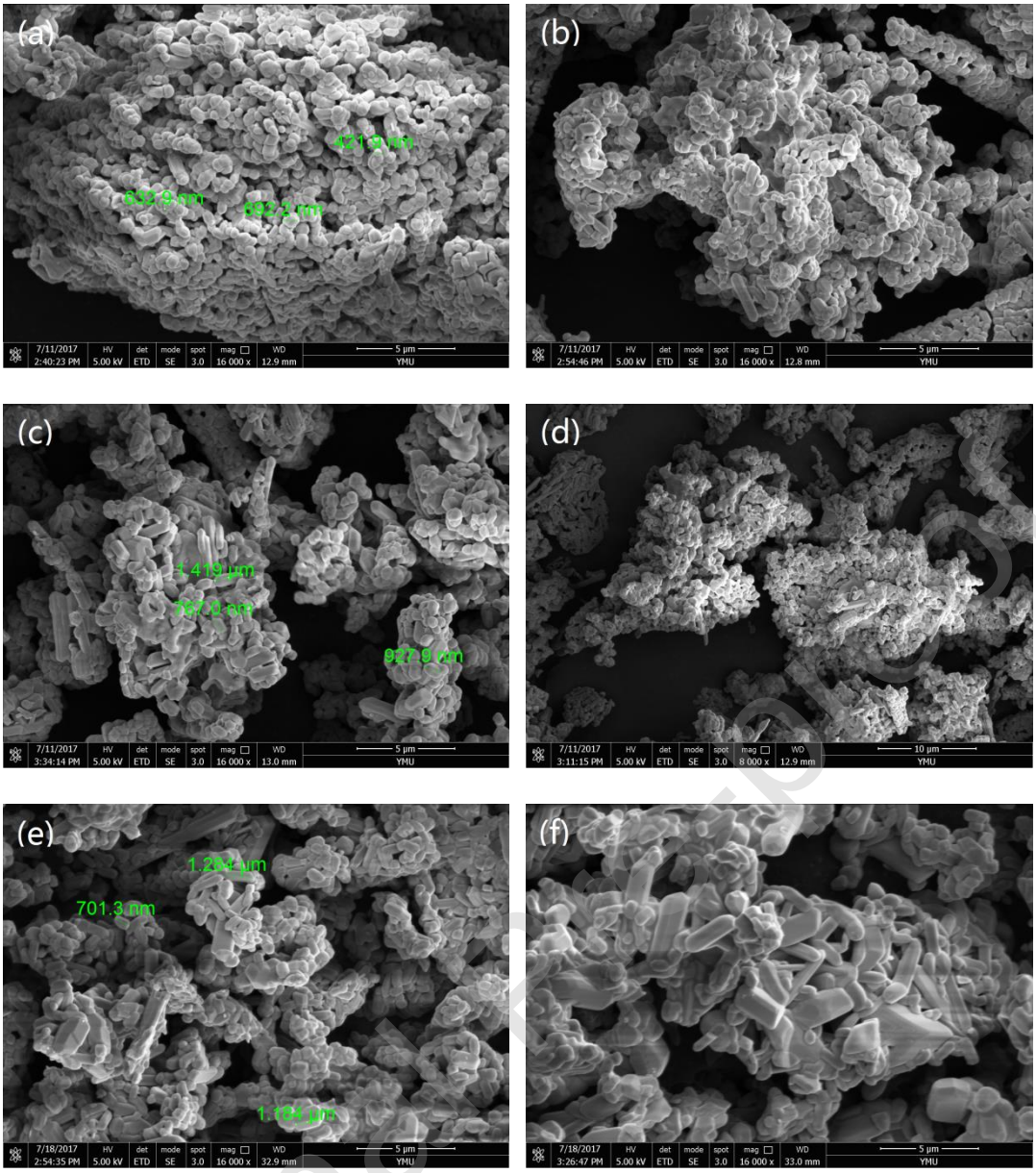

Fig. 6 SEM patterns of the final product under different calcination conditions, (a) 30 min; (b) 90 min; (c) 150 min; (d) 1233.15 K; (e) 1273.15 K; (f) 1323.15 K.

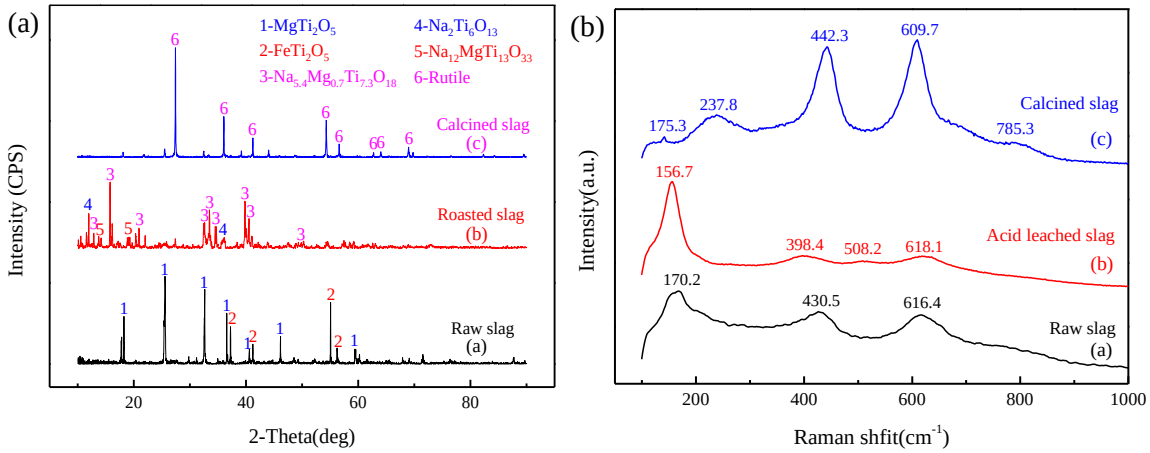

Fig. 7 XRD patterns and Raman spectra of samples at different stages, (a) XRD patterns; (b) Raman spectra

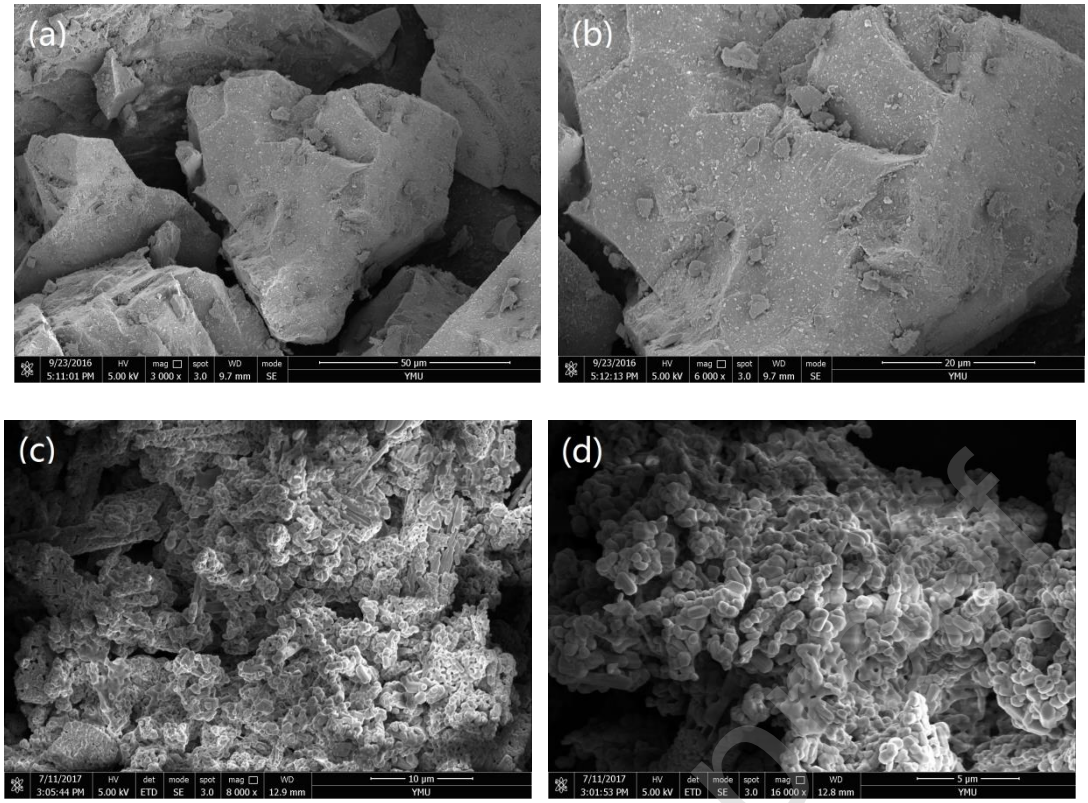

Fig. 8 SEM images of raw titanium slag and the final product, (a) raw titanium slag, 3000×; (b) raw titanium slag, 6000×; (c) the final product, 8000×; (d) the final product, 16000×.

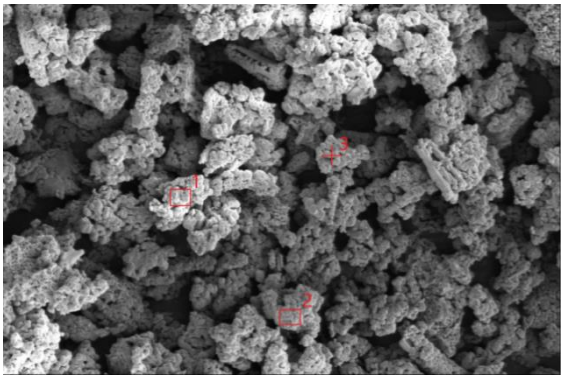

(a)

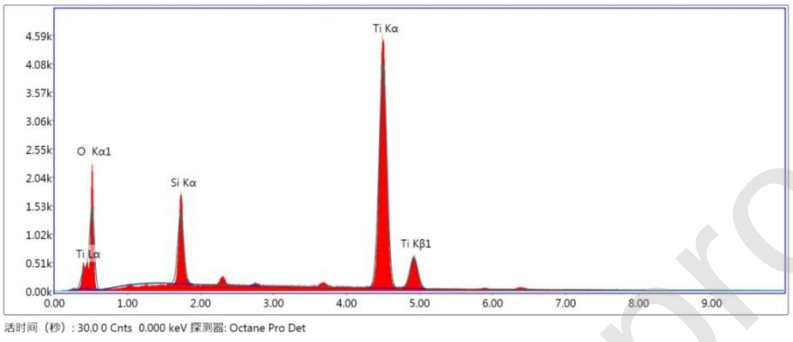

(b)

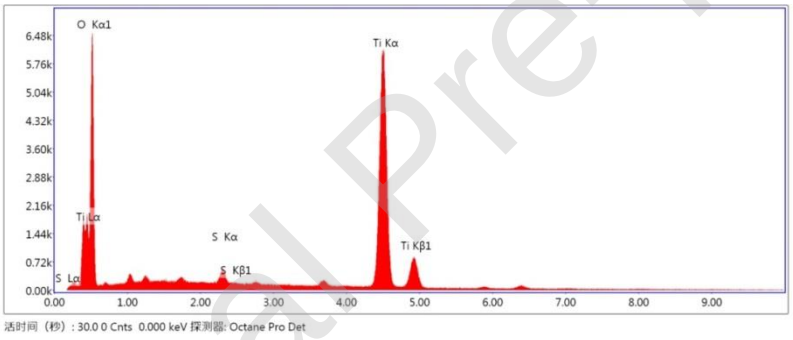

(c)

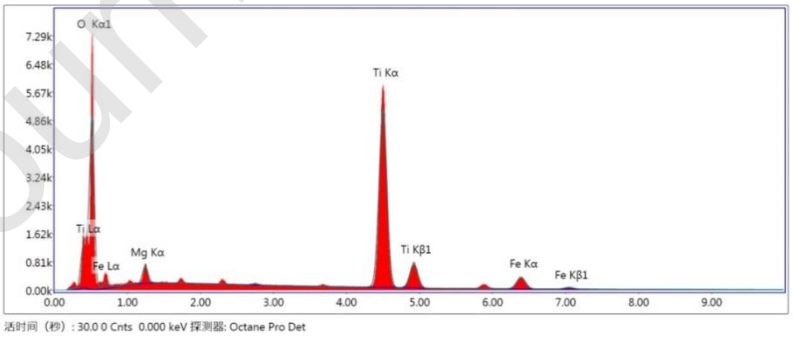

(d)

Fig. 9 EDAX spectra and (a) SEM image of the final product, (b) district 1; (c) district 2; (d) spot 3.